DOI: 10.19884/j.1672-5220.202406003

Interfacial Connection and Service Performance of CFRP-6061 Aluminum Alloy Enhanced by Laser-Plasma Co-Treatment

LIU Yang#, CHENG Lele#, LIU Yuhang, JIAO Zihe, ZHANG Jianxin, YU Muhuo, SUN Zeyu*
State Key Laboratory of Advanced Fiber Materials, Center for Civil Aviation Composites, College of Materials Science and Engineering, Donghua University, Shanghai 201620, China

Abstract: Carbon fiber reinforced polymer (CFRP)-aluminum alloys have the advantages of both CFRP and aluminum alloys, but their different properties make the connection challenging. In this study, the response surface method (RSM) was used to optimize the laser and plasma processing parameters for treating the 6061 aluminum alloy (AA 6061) surface. The AA 6061 surface was subjected to laser-plasma co-treatment with the optimized parameters. The CFRP-AA 6061 were prepared by the co-curing method. The interface properties of the CFRP-AA 6061 were evaluated by using the climbing drum peel (CDP) test. The single lap layer shear (SLLS) strengths of different treatment procedures under different service aging conditions were investigated. The optimal laser processing parameters included a laser scanning line spacing of 0.115 mm, a laser scanning rate of 102.719 mm/s and a laser frequency of 10.763 kHz, resulting in an average peel strength of 103.76 (N · mm)/mm. The optimal plasma processing parameters included a gas flow rate of 597.383 L/h, a processing distance of 5.821 mm and a processing time of 173.132 s, resulting in an average peel strength of 66.39 (N · mm)/mm. Under the optimal laser-plasma co-treatment condition, the average peel strength can reach 113.02 (N · mm)/mm, and the interfacial connection is better under different service aging conditions. This research can provide a reference for the interface treatment of composite-metal heterogeneous connections.

Keywords: carbon fiber reinforced polymer (CFRP); 6061 aluminum alloy (AA 6061); composite material; laser; plasma; service aging; heterogeneous connection
CLC number: R778 **Document code**: A
Article ID: 1672-5220(2025)04-0358-13

Open Science Identity (OSID)

0 Introduction

In the current development of lightweight technologies, achieving component performance and low cost by using a single-material design approach is challenging. Carbon fiber reinforced polymer (CFRP)-metal hybrid materials integrate the performance advantages of CFRP and metals, such as high specific strength and stiffness, excellent fatigue resistance, high damage tolerance, lightweight and efficient energy absorption performance[1-3]. These materials ensure overall strength while meeting lightweight requirements, with better performance than metals and lower costs than composites. They can provide important technical support for high-performance products and have excellent application potential in the automotive and aviation industries[4-6]. However, metals and CFRP differ in their thermal expansion coefficients and other physicochemical properties[7], and consequently, there are significant issues in the interfacial connection. Improving the performance of the interfacial connection between the metal and CFRP is important because the connection quality is closely related to the material application. The strength and reliability of the interfacial connection between two heterogeneous materials are usually improved by optimizing the connection mode and the surface treatment.

Mechanical treatment, such as sandblasting and grinding, is the primary approach for treating the metal surface. However, it usually requires heavy machinery, produces dust and debris, and is time-consuming and costly[8-10]. In contrast, laser surface treatment is a modern technology that can effectively improve the interlayer mechanical properties of CFRP-metal composites[11-15]. During laser etching, the high-energy laser beam causes instantaneous melting and vaporization of the metal surface, generating microscale features (e.g., holes and grooves) that solidify upon cooling[16]. These morphologies change the roughness and wettability of the metal surface and have different effects on the mechanical properties of the interface of heterogeneous materials[17]. Plasma treatment works based on the fundamental principle of exciting electrons, atoms, molecules and free radicals with ionized gas and generating jets under high

Received date: 2024-06-12
Foundation items: Fundamental Research Funds for the Central Universities, China (223202023G-23); Funds of State Key Laboratory of Advanced Fiber Materials, China (KF2203)
* Correspondence should be addressed to SUN Zeyu, email: sunzeyu@dhu.edu.cn
# These authors contributed equally to this work
Citation: LIU Y, CHENG L L, LIU Y H, et al. Interfacial connection and service performance of CFRP-6061 aluminum alloy enhanced by laser-plasma co-treatment [J]. *Journal of Donghua University (English Edition)*, 2025, 42(4): 358-370.

pressures to treat the surface of materials[18-19]. Air ionization involves the deposition of a large number of active particles onto the surface of a material, inducing various changes such as cleaning, etching, surface activation and cross-linking. Moreover, active particles generate high-energy polar groups on the surface of the material, which combine with the introduced free radicals to form new functional groups, thereby significantly improving the infiltration and adhesion of the material, increasing its surface energy, and enhancing its binding strength[20-22]. Plasma treatment is simple, environmentally friendly, efficient and widely used in bonded surface pretreatment[23-24].

Bonding[25], co-curing[26] and mechanical connection are effective methods for connecting metals and non-metallic materials. These methods are currently prevalent in the connection of metals and CFRP. Co-curing is a method in which uncured composite material layers and metal materials are cured simultaneously during a curing cycle. Applying the co-curing process to connection technology can significantly reduce the number of parts and the cost of assembling structural parts[27]. Furthermore, the elevated temperature during co-curing facilitates sufficient resin penetration into the microstructure of the metal surface and helps maintain an excellent layering structure.

This work presents a composite material composed of 6061 aluminum alloy (AA 6061) and CFRP, designated as CFRP-AA 6061, based on a co-curing integrated connection. Laser and plasma treatments are applied to the surface of AA 6061 to improve the connection performance. A response surface experiment is designed by using the Box-Behnken design (BBD)[28-30] to investigate the optimal process parameters and examine the influence of the process parameters of the two treatment methods on the connection performance of AA 6061. The effects of laser and plasma treatments on the service aging resistance of CFRP-AA 6061 composites are investigated. This work aims to provide a useful reference for the connection properties of CFRP-metal composites.

1 Experimental Design and Methods

1.1 Materials and fabrication

AA 6061 and T700-12K carbon fiber plain prepregs used in this work were sourced from Jiangsu Annansai Metal Products Co., Ltd. (China) and TORAY Co., Ltd. (China), respectively. The surface of AA 6061 was treated by using an atmospheric-pressure plasma system with an excitation frequency of 18 kHz, a high voltage of 5 kV, and a power output of 1 kW. The operating current and pulse width of the laser treatment for the AA 6061 surface were 1 A and 1 μs, respectively. The scanning angle was set at ± 45°.

The CFRP-AA 6061 sample was co-cured by using a vacuum bag compression process. To reduce the residual thermal stress of the laminates, three-stage curing was adopted. The heat preservation was conducted at 100, 130 and 150 ℃, and the corresponding durations were 60, 30 and 30 min, respectively. The heating and cooling rates were both 2 ℃/min. The co-curing process is illustrated in Figs. 1(a) and 1(b). After cooling to room temperature, the cured CFRP-AA 6061 was obtained. To investigate the effects of laser treatment, plasma treatment and their combination on CFRP-AA 6061, the AA 6061 surface was subjected to laser treatment, plasma treatment and laser-plasma co-treatment with the optimized parameters, respectively. The corresponding CFRP-AA 6061 samples are denoted as LTS, PTS and CTS, respectively, and the CFRP-AA 6061 sample made of untreated AA 6061 is denoted as UTS.

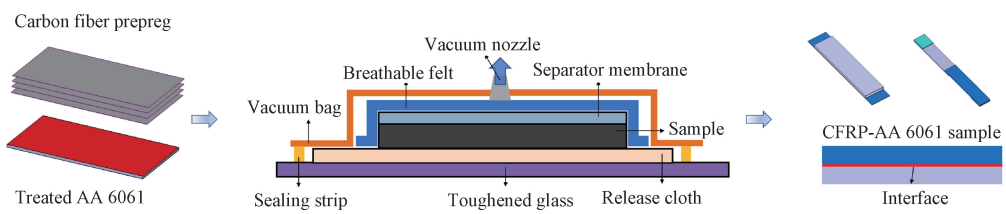

(a)

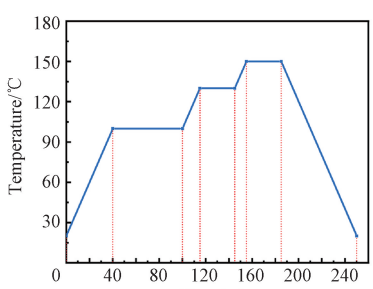

(b)

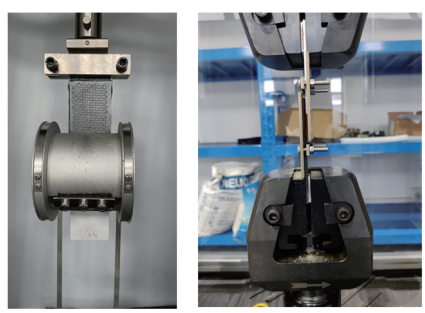

(c)

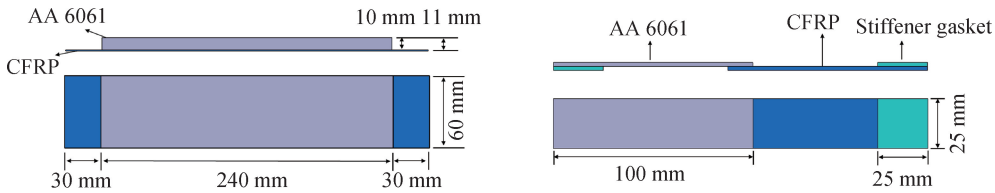

(d)

Fig. 1 Preparation and experimental process of CFRP-AA 6061 sample: (a) curing process; (b) curing temperature curve; (c) devices for climbing drum peel (CDP) test (left) and single lap layer shear (SLLS) test (right); (d) sample sizes

1.2 Response surface method (RSM)

It is difficult to determine the optimal laser processing parameters by using the single-factor test method, necessitating further investigation of the relationships and interactions between these parameters. Therefore, a multi-parameter and multi-level orthogonal experimental scheme is required. RSM is a mathematical approach that integrates optimization design and statistical analysis. It can optimize the process parameters by designing an experimental scheme and analyzing the functional relationship between the response value and the model. The Box-Behnken design (BBD) is a design option for RSM. BBD produces representative results while simplifying the experimental schemes. In this work, BBD was used to study the experimental parameters of laser and plasma treatments of AA 6061 surfaces and the effects of their interactions on the interfacial connection of CFRP-AA 6061. The three parameters for laser processing (laser frequency A_L, scanning rate B_L and scanning line spacing C_L) and the three parameters for plasma processing (processing time A_P, processing distance B_P and gas flow rate C_P) were set at different levels (−1 for low, 0 for medium and +1 for high), and the peel strength was defined as a response variable. The three independent experimental parameters selected for the two processing methods and their respective levels are listed in Table 1.

Table 1 Experimental factor levels of laser and plasma treatments

Parameter of laser treatment	Level			Parameter of plasma treatment	Level		
	−1	0	+1		−1	0	+1
A_L/kHz	10	20	30	A_P/s	10	110	210
B_L/(mm/s)	100	300	500	B_P/mm	5.0	12.5	20.0
C_L/mm	0.1	0.3	0.5	C_P/(L/h)	500	550	600

1.3 CDP test

According to GB/T 1457—2022 standard, the samples were tested by using a microcomputer-controlled electronic universal testing machine (Metz Industrial Systems Co., Ltd., China) (Fig. 1(c)) with a 25 mm/min loading speed. In the sample, the CFRP layer was the peeled panel, and the AA 6061 profile was the unpeeled panel. The AA 6061 panel size was 240 mm × 60 mm × 10 mm, and the CFRP panel size was 300 mm × 60 mm × 1 mm, as presented in Fig. 1(d). The average peel strength is calculated by

$$M = \frac{(P_m - P_0)(D - d + t_b - t_f)}{2b}, \quad (1)$$

where M, P_m, P_0, D, d, b, t_b and t_f represent the average peel strength, average peeling load, resistance load, drum flange diameter, drum diameter, sample width, peeled panel thickness and loaded tape thickness, respectively. Here, the average peel strengths for laser treatment and plasma treatment are denoted as M_{laser} and M_{plasma}, respectively.

1.4 SLLS test

SLLS tests were performed following the ASTM D3165—07 standard to examine the effects of temperature, humidity and salt spraying on the aging process. SLLS strength was used to characterize the interface bonding properties of the CFRP-AA 6061 at different time of salt spray aging. The sample was spline-bonded, and the interfacial connection area was 12.5 mm × 25 mm as shown in Fig. 1(d). An SLLS testing machine (Metz Industrial Systems Co., Ltd., China) (Fig. 1(c)) was used to test the lap spline, and the tensile rate of the samples was 2 mm/min. Five samples were tested in each group, and the average value was calculated. The SLLS strength of the lap joint is calculated by

$$\tau = \frac{F}{b \times l}, \quad (2)$$

where τ, F and l are the SLLS strength, maximum load of sample shear failure and length of sample overlap, respectively.

1.5 Service aging

The lap aging behavior of the interface between CFRP and AA 6061 was investigated in service environments: a salt spray corrosion test chamber, a hot and cold shock experiment box and a constant temperature and humidity box. In the treatment

parameters of each aging test, the mass concentration of sodium chloride in the salt spray aging test was 50 g/L (Fig. 2(a)). In the high- and low-temperature aging tests, the high temperature was 80 ℃, the low temperature was −40 ℃, and the cycle duration was 72 min (Fig. 2(b)).

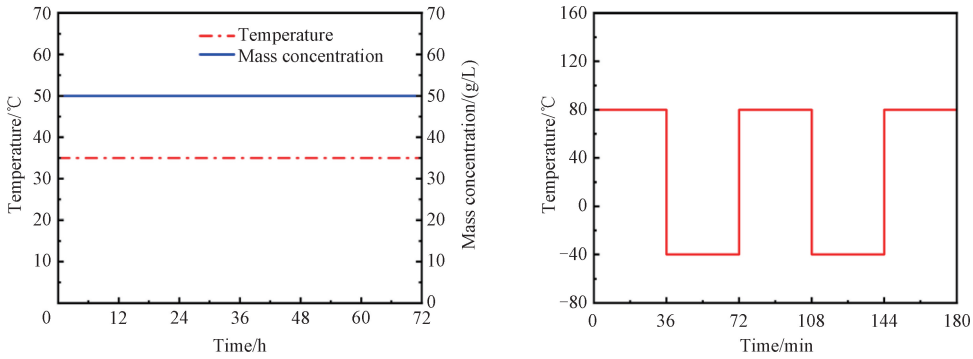

Fig. 2 Environmental aging test processing parameters: (a) salt spray aging; (b) high- and low-temperature aging

2 Results and Discussion

2.1 Optimization of BBD

2.1.1 Interface characteristics of CFRP-AA 6061 based on RSM

The relationship between the interfacial connection of the CFRP-AA 6061 and laser/plasma process parameters was studied by using RSM. The results of the orthogonal experiments designed by using BBD in Design-Expert software are presented in Table 2.

After regression fitting the experimental findings in Table 2, model equations can be obtained:

$$M_{laser} = 130.066\,62 - 0.145\,6A_L - 0.105\,591B_L - 148.835C_L + 0.000\,087A_LB_L + 0.711\,25A_LC_L + 0.023\,215B_LC_L - 0.010\,173A_L^2 + 0.000\,107B_L^2 + 119.943\,75C_L^2, \quad (3)$$

$$M_{plasma} = 1\,456.231\,80 - 0.201\,581A_P + 7.685\,20B_P - 5.605\,27C_P - 0.003\,974A_PB_P + 0.000\,483A_PC_P - 0.017\,393B_PC_P + 0.000\,229A_P^2 + 0.048\,611B_P^2 + 0.005\,478C_P^2. \quad (4)$$

Table 2 Orthogonal experimental results of surface treatment parameters of AA 6061

No.	Parameter of laser treatment			M_{laser}/[(N·mm)/mm]	Parameter of plasma treatment			M_{plasma}/[(N·mm)/mm]
	A_L	B_L	C_L		A_P	B_P	C_P	
1	20	100	0.5	78.51	110	12.5	550	18.79
2	20	500	0.5	64.82	210	5.0	550	39.13
3	20	300	0.3	74.81	210	12.5	600	55.55
4	30	300	0.5	65.77	10	20.0	550	14.44
5	30	300	0.1	84.68	110	5.0	600	66.06
6	20	500	0.1	85.78	110	12.5	550	18.34
7	20	300	0.3	73.46	10	12.5	600	39.29
8	10	300	0.5	68.06	110	20.0	600	30.27
9	30	100	0.3	78.82	110	12.5	550	18.58
10	10	500	0.3	75.34	110	20.0	500	17.42
11	10	300	0.1	92.66	110	12.5	550	19.03
12	30	500	0.3	68.31	10	5.0	550	18.82
13	20	300	0.3	73.93	210	12.5	500	25.42
14	20	300	0.3	74.54	110	12.5	550	19.19
15	10	100	0.3	86.55	10	12.5	500	18.81
16	20	100	0.1	103.17	210	20.0	550	22.83
17	20	300	0.3	73.32	110	5.0	500	27.12

The experimental model obtained in Table 2 was subjected to analysis of variance (ANOVA) to assess the influence of various factors associated with the laser and plasma treatments on the response value, and the

interaction analysis results are presented in Tables 3 and 4. In variance statistics, when the p-value of the model item is less than 0.05, the model item is significant, whereas the model item is non-significant when the p-value is higher than 0.10. As shown in Tables 3 and 4, the ANOVA results for laser treatment and plasma treatment indicate that the process parameters significantly influence the average peel strength. In laser treatment, the relative influence weights of each factor on the average peel strength follow the descending order: laser scanning line spacing C_L, laser scanning rate B_L, laser frequency A_L; while in plasma treatment, the corresponding weights follow the descending order: gas flow rate C_P, processing distance B_P, processing time A_P.

Table 3 ANOVA results and model summary statistics for the fitted quadratic polynomial model of CDP test results after laser treatment

Source	Sum of squares	Degree of freedom	Mean square	F-value	p-value	Statistic	Value
Model	1 609.14	9	179.50	79.86	< 0.000 1	SD	1.50
A_L	78.31	1	78.31	34.84	0.0006	Mean	77.80
B_L	348.48	1	348.48	155.04	<0.000 1	C. V%	1.93
C_L	993.02	1	992.02	441.80	<0.000 1	PRESS	227.11
A_LB_L	0.12	1	0.12	0.054 5	0.822 1	R^2	0.990 4
A_LC_L	8.09	1	8.09	3.60	0.099 5	Adj R^2	0.978 0
B_LC_L	3.42	1	3.42	1.52	0.257 0	Pred R^2	0.860 8
A_L^2	4.36	1	4.36	1.94	0.206 5	Adequate precision	33.996 6
B_L^2	76.42	1	76.42	34.00	0.000 6		
C_L^2	96.92	1	96.92	43.12	0.000 3		
Residual error	15.74	7	2.25	—	—		
Lack of fit	14.03	3	4.68	10.96	0.021 2		
Pure error	1.71	4	0.43	—	—		
Total	1 624.88	16	—	—	—		

Notes: SD denotes the standard deviation; C. V% denotes the coefficient of variation; PRESS denotes the predicted residual error sum of squares; R^2 denotes the determination coefficient; Adj R^2 denotes the adjusted determination coefficient; Pred R^2 denotes the predicted determination coefficient.

Table 4 ANOVA results and model summary statistics for the fitted quadratic polynomial model of CDP test results after plasma treatment

Source	Sum of squares	Degree of freedom	Mean square	F-value	p-value	Statistic	Value
Model	3 262.89	9	367.02	31.43	< 0.000 1	SD	3.42
A_P	332.32	1	332.32	28.46	0.001 1	Mean	27.59
B_P	547.49	1	547.49	46.88	0.000 2	C. V%	12.38
C_P	1 310.97	1	1 310.97	112.25	<0.000 1	PRESS	1 301.28
A_PB_P	35.53	1	35.53	3.04	0.124 6	R^2	0.975 8
A_PC_P	23.29	1	23.29	1.99	0.200 8	Adj R^2	0.944 8
B_PC_P	170.17	1	170.17	14.57	0.006 6	Pred R^2	0.615 6
A_P^2	21.99	1	21.99	1.88	0.212 3	Adequate precision	19.359 9
B_P^2	31.48	1	31.48	2.70	0.144 6		
C_P^2	789.65	1	789.65	67.61	<0.000 1		
Residual error	81.75	7	11.68	—	—		
Lack of fit	81.28	3	27.09	232.47	<0.000 1		
Pure error	0.47	4	0.12	—	—		
Total	3 344.64	16	—	—	—		

The R^2 and Adj R^2 values of the laser processing model are 0.990 4 and 0.978 0, respectively, and those of the plasma processing model are 0.975 8 and 0.944 8, respectively, which are close to 1, indicating the statistical significance of the models. The adequate precision values of the laser treatment model (33.996 6) and plasma treatment model (19.359 9) are significantly higher than the value of 4 (4 indicates that the model is desirable), which proves that the model is highly reliable. As calculated by Eqs. (3) and (4), when the laser processing parameters are 10.763 kHz, 102.719 mm/s and 0.115 mm, the M_{laser} reaches a maximum value of 103.17 (N · mm)/mm; when the plasma processing parameters are 173.132 s, 5.821 mm and 597.383 L/h, the M_{plasma} reaches a maximum value of 66.36 (N · mm)/mm.

2.1.2 Interactive effects of variables

The two-dimensional (2D) average peel strength response surfaces obtained by using Design-Expert software are illustrated in Figs. 3 and 4. In the response surface diagram, variables other than the axes are kept at the center level. The effects of individual parameters and interactions on the interface properties can be obtained by using a 2D elliptic contour diagram.

Figure 3(a) illustrates the interactive effects of laser frequency and scanning rate on the average peel strength in laser processing with a scanning line spacing of 0.10 mm. In the process of scanning rate reduction, the lower the laser frequency, the higher the average peel strength. When the scanning rate is sufficient to satisfy the treatment effect of laser processing, processing parameters with low laser frequency and high scanning rate can ensure a high average peel strength and improve processing efficiency. The response surface diagram of the laser frequency and scanning line spacing at a constant scanning rate of 100 mm/s is depicted in Fig. 3(b). The average peel strength can be improved by reducing scanning line spacing and laser frequency. However, the improvement effect from laser frequency reduction becomes less pronounced when the scanning line spacing is sufficiently small to cause the laser trace to be closer. Figure 3(c) demonstrates the interactive effects of the scanning rate and scanning line spacing on the average peel strength at a laser frequency of 20 kHz. The proximity of the contour line to a circle indicates that the scanning rate and scanning line spacing at this laser frequency have comparable and significant effects on the average peel strength. When the laser frequency is maintained at a suitable value, the interface bonding properties can be improved by reducing the scanning rate and scanning line spacing, and the two parameters have a high degree of equivalence.

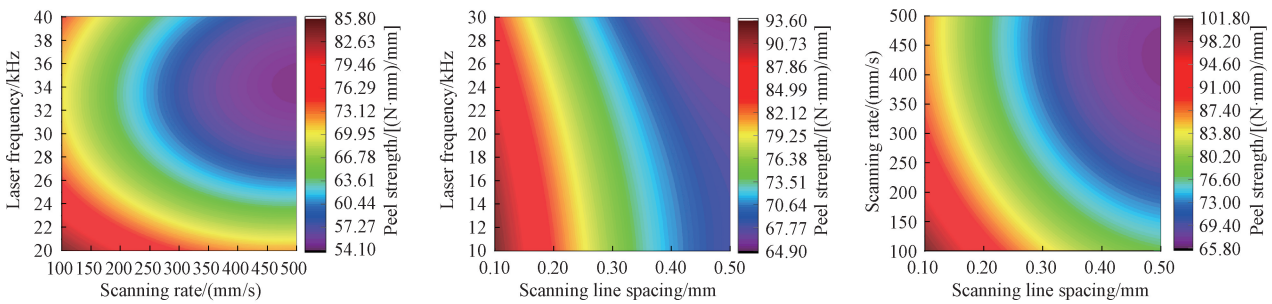

Fig. 3 2D response surface plots of different laser processing parameters: (a) laser frequency vs. scanning rate; (b) laser frequency vs. scanning line spacing; (c) scanning rate vs. scanning line spacing

The interactive effects of the processing time and distance on the interface properties when the plasma gas flow rate is maintained at 550 L/h during plasma processing are presented in Fig. 4(a). There is an apparent interaction between the plasma processing time and distance. When the time increases from 10 to 210 s, the average peel strength increases as the processing distance decreases. The average peel strength exhibits a temporal increase as the processing distance decreases from 20.0 to 5.0 mm. The contours indicate that the influence of the processing time and distance on the average peel strength is essentially the same, implying that an increase in the processing time and a decrease in the processing distance are equivalent. Figure 4(b) depicts the contours and response surfaces of the processing time and gas flow rate when the processing distance is 12.5 mm. It can be observed that when the processing time increases from 10 to 210 s, the increase in the average peel strength is less than that when the gas flow rate increases from 500 to 600 L/h. This indicates that the gas flow rate has a more significant effect on the average peel strength compared to the processing time. The interaction effect of the gas flow rate and processing distance on the interface properties at a processing time of 110 s is presented in Fig. 4(c). The elliptical distribution pattern in Fig. 4(c) demonstrates that the gas flow rate is the more critical parameter affecting the peel strength. When the processing distance decreases from 20.0 to 5.0 mm, the average peel strength shows an upward trend with increasing the gas flow rate.

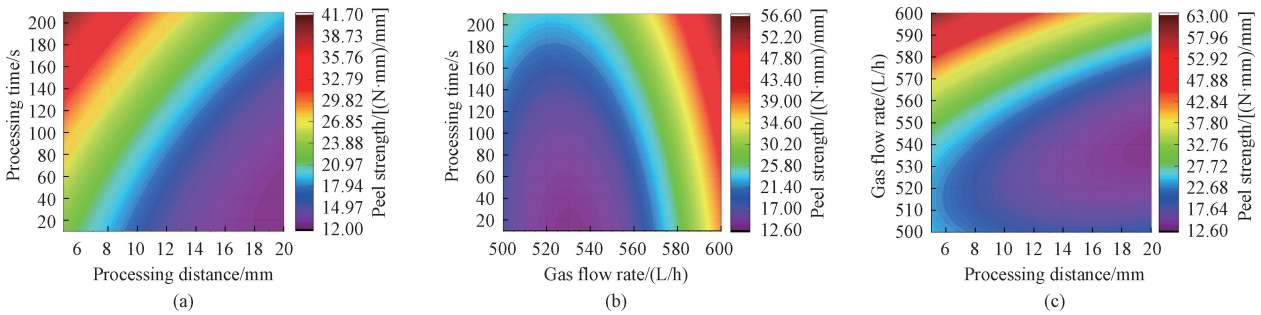

Fig. 4 2D response surface plots of different plasma processing parameters: (a) processing time vs. processing distance; (b) processing time vs. gas flow rate; (c) gas flow rate vs. processing distance

Moreover, due to the processing distance limit of the machine-emitted plasma, when the distance between the nozzle and sample surface is too large, the plasma cloud cannot effectively reach the AA 6061 surface, thereby impeding interface performance enhancement. However, an inadequate processing distance may cause excessive ablation and high material surface temperatures, negatively affecting interface bonding properties. Therefore, a moderate processing distance is recommended.

2.2 Effect of laser-plasma co-treatment on CFRP-AA 6061

Figure 5 represents the interface properties of the CFRP-AA 6061 after different treatment methods. It illustrates four conditions for the AA 6061 surface: untreated, optimal plasma treatment, optimal laser treatment and laser-plasma co-treatment. As indicated in Fig. 5(a), the average peel strengths under the above conditions are 7.01, 66.39, 103.76 and 113.02 (N·mm)/mm, respectively. This shows that the effect of laser-plasma co-treatment is the best.

Scanning electron microscopy (SEM) was used to observe the surface of the AA 6061 treated in different ways. Figure 6(a) shows that the surface of the untreated AA 6061 is relatively smooth. An oxide film formed on the AA 6061 surface after plasma treatment. Laser treatment rapidly increased the surface temperature and thus caused ablation, which left a ±45° notch topography and created highly regular pits. After laser-plasma co-treatment, the AA 6061 surface exhibited both the ±45° notch pit morphology from laser treatment and the oxide film morphology from plasma treatment. This hybrid structure significantly enhances the interface bonding force of CFRP-AA 6061 composites.

The surface morphology and roughness of AA 6061 under different surface treatments are illustrated in Figs. 6(b) and 5(b), respectively. It can be observed that plasma treatment not only forms an oxide layer on the AA 6061 surface but also enhances roughness through ablation effects.

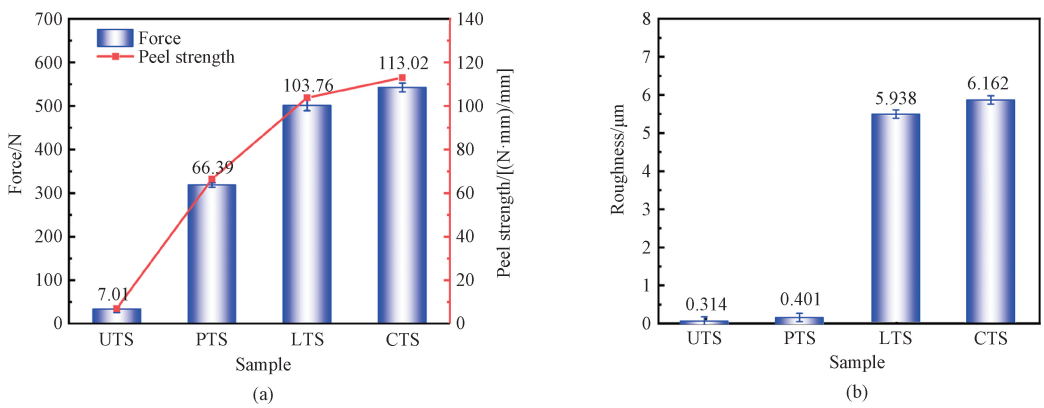

Fig. 5 Interface properties of CFRP-AA 6061 with different surface treatments: (a) mechanical properties; (b) surface roughness

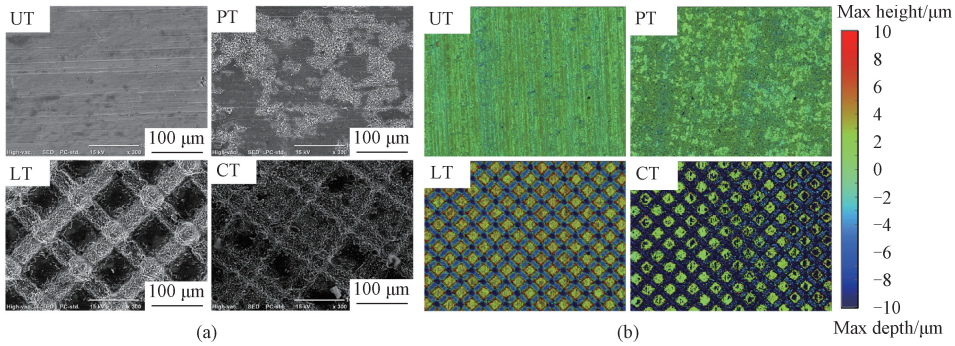

UT—untreated; PT—plasma treatment; LT—laser treatment; CT—laser-plasma co-treatment.

Fig. 6 Surface morphology of AA 6061 with different surface treatments: (a) SEM images; (b) harshness topographies

Laser-plasma co-treatment produces an AA 6061 surface characterized by laser-induced roughness, along with an oxidation layer and ablation features from the plasma treatment. The regular microgrooves and the increased surface roughness enhance the mechanical interlocking during co-curing bonding between the AA 6061 and CFRP. Consequently, the interface bonding properties improve, with the average peel strength showing significant enhancement along with surface roughness.

According to surface energy theory[31-32], an optimal interface requires the bonding resin to fully wet and penetrate the substrate surface. The surface energy of AA 6061 can be calculated by using the two-liquid method. The water contact angle (WCA) and ethylene glycol contact angle (GCA) were measured. Table 5 lists the surface energy data of the AA 6061 surface under different surface treatments. The untreated AA 6061 has slight hydrophobicity due to the oxide film. Its WCA and GCA are 94.62° and 113.30°, respectively, and its dispersion component γ_{Sd}, polar component γ_{Sp} and total surface free energy γ_S are 3.26, 34.42, and 37.68 mJ/m^2, respectively.

After different surface treatments, the wettability of the AA 6061 surface changed greatly (Table 5). Laser treatment on AA 6061 surfaces causes significantly greater reductions in WCA and GCA than plasma treatment. Laser-plasma co-treatment demonstrates the most substantial contact angle reduction, resulting in superior wettability enhancement compared to individual surface treatments.

Table 5 Surface contact angle and surface energy of AA 6061 under different treatments

Surface treatment	WCA/(°)	GCA/(°)	γ_{Sd}/(mJ/m^2)	γ_{Sp}/(mJ/m^2)	γ_S/(mJ/m^2)
Untreated	94.62	113.30	3.26	34.42	37.68
Plasma treatment	46.83	85.37	13.07	119.86	132.94
Laser treatment	23.93	73.58	12.08	144.68	156.76
Laser-plasma co-treatment	16.46	72.07	13.07	152.49	165.56

The influence trend of different surface treatments on the contact angle and surface energy is consistent, indicating that both laser treatment and plasma treatment changed the micro-hydrophobic state of the AA 6061 surface and improved the overall wettability and surface energy of AA 6061. Consequently, the interfacial connection of the CFRP-AA 6061 was improved.

2.3 Effect of environmental aging on interface bonding properties of CFRP-AA 6061

Metal- and fiber-reinforced composite structures can be widely used in aircraft, automobiles, ships, railway vehicles, and civil and electronic sectors. The connection structures must remain stable for 5 – 30 years during service. During this time, they are affected by various environmental factors such as temperature, humidity and salt spray, resulting in a reduction in material performance or even damage, thereby changing the failure mode.

2.3.1 Effect of salt spray aging on failure of CFRP-AA 6061 interface

Salt spray corrosion is an atmospheric corrosion characterized by severe destructive corrosion. It is caused by the electrochemical reaction between the metal and chloride ions in the salt spray through the surface of the material, which causes destructive corrosion. The properties of the material change after corrosion, and the service life is affected. Figure 7(a) presents the SLLS strength of the CFRP-AA 6061 after salt spray aging for 0 (unaged), 24, 48 and 72 h. It is observed that with an increase in the salt spray aging time, the SLLS strength of the samples progressively decreases. This is because, with the increase in corrosion time, more corrosive media infiltrate the interior of the sample, degrading the interface between the CFRP and AA 6061, and causing a reduction in SLLS strength. It is commonly required that after 24 h of salt spray testing, the adhesion retention rate should be

higher than 80%. For high-performance or critical applications, a retention rate higher than 90% is often targeted. After aging for 24 h, the SLLS strengths of PTS, LTS and CTS decrease by 52.47%, 11.49% and 8.79%, respectively, indicating that the sample after laser-plasma co-treatment has excellent corrosion resistance. After aging for 72 h, the SLLS strengths of PTS, LTS and CTS decrease by 85.65%, 34.87% and 21.83%, respectively, indicating that the corrosion resistance of the laser-plasma co-treated sample is the best under the long-term salt spray aging environment. As shown in Fig. 7(b), the strength of the PTS decreases most significantly under high- and low-temperature aging. After aging for 30 d, the SLLS strength of UTS decreases by approximately 67.86%. In comparison, the SLLS strengths of LTS and CTS decrease by 15.68% and 15.60%, respectively, over the same aging time. Therefore, LTS and CTS have excellent high- and low-temperature aging resistance.

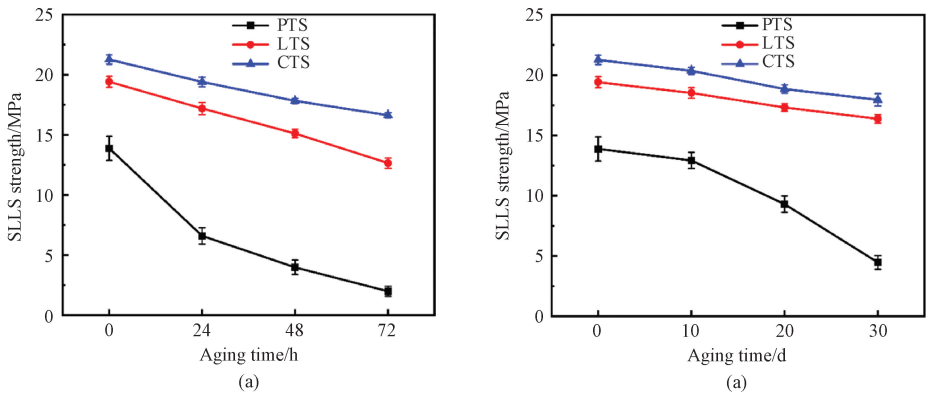

Fig. 7 SLLS strength of CFRP-AA 6061 interface under different aging: (a) salt spray aging; (b) high- and low-temperature aging

Figure 8 illustrates the failure sections of the lap joints under different salt spray aging times. After aging, the PTS lap joints gradually transform into a mixed mode of cohesive and interface failure and a full interface failure mode, significantly reducing the interface strength and even causing interface debonding owing to the test preload. Interface failure is observed in the LTS and CTS lap joints after aging. After aging for 72 h, a large area of interface failure develops, accompanied by a significant decrease in SLLS strength. This phenomenon can be attributed to the infiltration of the corrosive medium into the interior of the material during salt spray aging. The electrochemical reaction occurs with aluminum, resulting in interface failure. In contrast, the corrosive medium may penetrate the fiber and resin interface of CFRP, causing the interface to hydrolyze or the resin to absorb water and swell, resulting in cohesive failure and strength loss. The comprehensive aging test results indicate that CTS can provide a higher SLLS strength in various aging environments to ensure the safety and reliability of the lap joint.

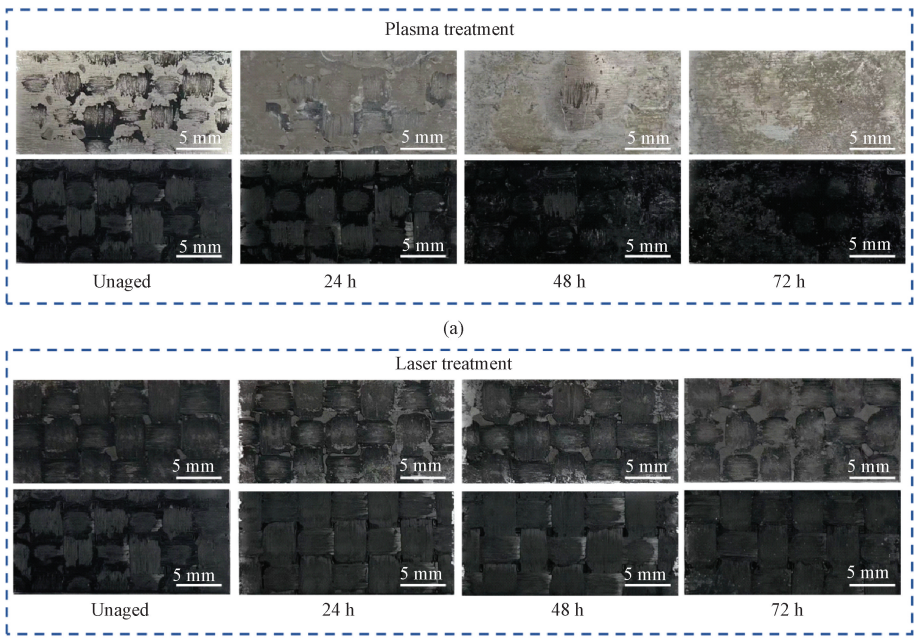

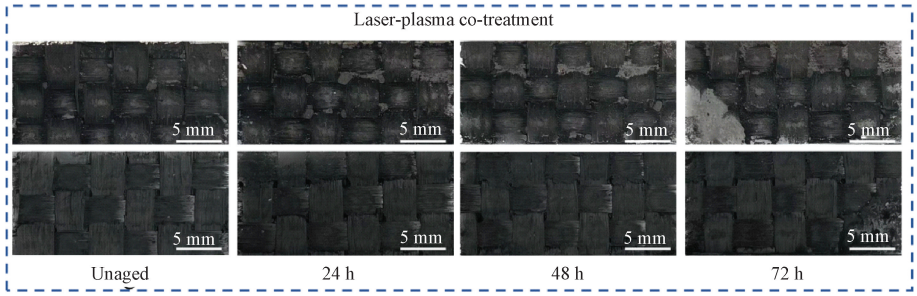

Fig. 8 Failure sections of CFRP-AA 6061 lap joints before and after salt spray aging: (a) PTS; (b) LTS; (c) CTS

2.3.2 Effect of high- and low-temperature aging on failure of CFRP-AA 6061 interface

The failure sections of the CFRP-AA 6061 lap joint after 0, 10, 20, and 30 d of high- and low-temperature aging are displayed in Fig. 9. Cohesive failure and fiber tear failure characterize the unaged state of the lap joint. When the lap joint is aged at high and low temperatures, the internal stress induced by the different thermal expansion coefficients between different materials leads to the failure mode of the PTS lap joint changing to cohesive and interface failure after aging for 10 d. The proportion of cohesive failure decreases with increasing aging time, indicating that the interface performance achieved by the plasma treatment is significantly affected by high- and low-temperature aging. After aging, the LTS and CTS lap joints exhibit a mixture of cohesive failure and fiber tear. The fiber tear area decreases, the cohesive failure area increases, and the SLLS strength decreases with an increase in the aging time. The fiber tear area of the CTS lap joint is always more significant than that of the LTS lap joint, demonstrating better interfacial bonding properties in the LTS.

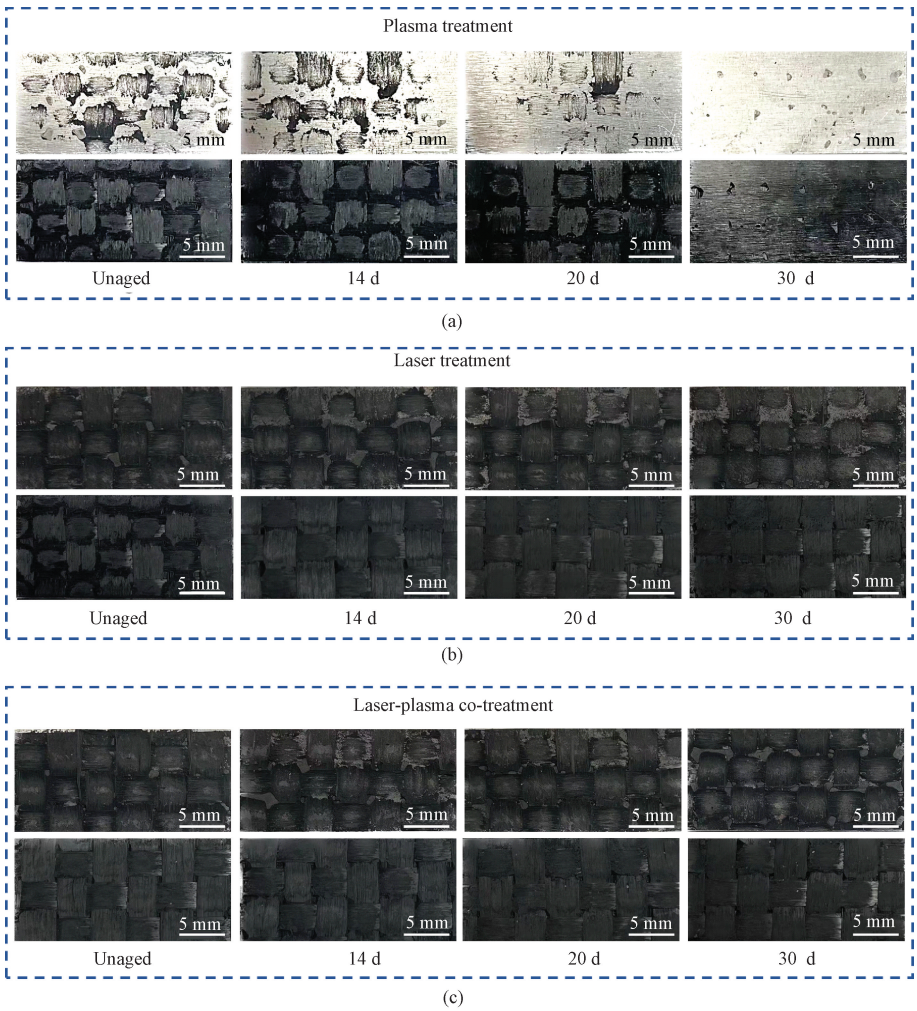

Fig. 9 Failure sections of CFRP-AA 6061 lap joints before and after high- and low-temperature aging: (a) PTS; (b) LTS; (c) CTS

3 Conclusions

This study used RSM to optimize the processing parameters of laser- and plasma-treated AA 6061 surfaces. Subsequently, laser-plasma co-treatment was performed on the AA 6061 surface with the optimized processing parameters, and the service aging resistance of the CFRP-AA 6061 interface after laser-plasma co-treatment was investigated. The following conclusions were drawn.

1) The optimal laser processing parameters after RSM optimization were a laser scanning line spacing of 0.115 mm, a laser scanning rate of 102.719 mm/s and a laser frequency of 10.763 kHz; the optimal plasma parameters were a gas flow rate of 597.383 L/h, a processing distance of 5.821 mm and a processing time of 173.132 s. Laser plasma co-treatment resulted in an AA 6061 surface that exhibited regular network pits of laser treatment and the oxide film and ablation state of the plasma treatment. Compared with the surface roughness and surface energy of a single treatment, the co-treatment had a more pronounced improvement effect, and the highest average peel strength of 113.02 (N · mm)/mm was achieved.

2) Under the optimal treatment parameters, the lap joint of CFRP-AA 6061 made of the laser-plasma co-treated AA 6061 exhibited excellent interfacial connection performance under salt spray and high- and low-temperature environments. After aging for 24 h in a salt spray environment, the SLLS strengths of PTS, LTS and CTS decreased by 52.47%, 11.49% and 8.79%, respectively. After high- and low-temperature aging for 30 d, the SLLS strengths of PTS, LTS and CTS decreased by 67.86%, 15.68% and 15.60%, respectively.

References

[1] FLEISCHER J, NIESCHLAG J. Introduction to CFRP-metal hybrids for lightweight structures [J]. *Production Engineering*, 2018, 12(2): 109-111.

[2] LI Z Y, ZHANG J Y, JACKSTADT A, et al. Low-velocity impact behavior of hybrid CFRP-elastomer-metal laminates in comparison with conventional fiber-metal laminates [J]. *Composite Structures*, 2022, 287: 115340.

[3] DAYNES S, WEAVER P. Analysis of unsymmetric CFRP-metal hybrid laminates for use in adaptive structures [J]. *Composites Part A: Applied Science and Manufacturing*, 2010, 41(11): 1712-1718.

[4] MEI Z H, PEI Z L, CHENG L L, et al. Impact behavior analysis and failure mode comparison of glass fiber (GF)/polydicyclopentadiene (PDCPD) thermosetting composite for automobile bottom protection plate [J]. *Journal of Donghua University (English Edition)*, 2024, 41(6): 595-606.

[5] KUNČICKÁ L, KOCICH R, LOWE T C. Advances in metals and alloys for joint replacement [J]. *Progress in Materials Science*, 2017, 88: 232-280.

[6] ZHANG X S, CHEN Y J, HU J L. Recent advances in the development of aerospace materials [J]. *Progress in Aerospace Sciences*, 2018, 97: 22-34.

[7] WANG Z, XIAN G J. Effects of thermal expansion coefficients discrepancy on the CFRP and steel bonding [J]. *Construction and Building Materials*, 2021, 269:121356.

[8] LU S K, HUA D X, LI Y, et al. Stiffness calculation model of thread connection considering friction factors [J]. *Mathematical Problems in Engineering*, 2019, 2019(1): 8424283.

[9] XIAO Y, ISHIKAWA T. Bearing strength and failure behavior of bolted composite joints (part Ⅰ: experimental investigation) [J]. *Composites Science and Technology*, 2005, 65(7/8): 1022-1031.

[10] WANG J, ZHANG G W, ZHENG X F, et al. A self-piercing riveting method for joining of continuous carbon fiber reinforced composite and aluminum alloy sheets [J]. *Composite Structures*, 2021, 259: 113219.

[11] PARDAL G, MECO S, DUNN A, et al. Laser spot welding of laser textured steel to aluminium [J]. *Journal of Materials Processing Technology*, 2017, 241: 24-35.

[12] ALFANO M, LUBINEAU G, FURGIUELE F, et al. Study on the role of laser surface irradiation on damage and decohesion of Al/epoxy joints [J]. *International Journal of Adhesion and Adhesives*, 2012, 39: 33-41.

[13] PAN Y C, WU G Q, HUANG Z, et al. Effects of surface pre-treatments on mode Ⅰ and mode Ⅱ interlaminar strength of CFRP/Mg laminates [J]. *Surface and Coatings Technology*, 2017, 319: 309-317.

[14] KURTOVIC A, BRANDL E, MERTENS T, et al. Laser induced surface nano-structuring of Ti-6Al-4V for adhesive bonding [J]. *International Journal of Adhesion and Adhesives*, 2013, 45: 112-117.

[15] LI Y Y, MENG S, GONG Q M, et al. Experimental and theoretical investigation of laser pretreatment on strengthening the heterojunction between carbon fiber-reinforced plastic and aluminum alloy [J]. *ACS Applied Materials & Interfaces*, 2019, 11(24): 22005-22014.

[16] BYSKOV-NIELSEN J, BOLL J V, HOLM A H, et al. Ultra-high-strength micro-mechanical

interlocking by injection molding into laser-structured surfaces [J]. *International Journal of Adhesion and Adhesives*, 2010, 30(6): 485-488.

[17] LEONE C, GENNA S. Effects of surface laser treatment on direct co-bonding strength of CFRP laminates[J]. *Composite Structures*, 2018, 194: 240-251.

[18] BÓNOVÁ L, ZHU W K, PATEL D K, et al. Atmospheric pressure microwave plasma for aluminum surface cleaning [J]. *Journal of Vacuum Science & Technology A: Vacuum, Surfaces, and Films*, 2020, 38(2): 023002.

[19] MUÑOZ J, BRAVO J A, CALZADA M D. Aluminum metal surface cleaning and activation by atmospheric-pressure remote plasma [J]. *Applied Surface Science*, 2017, 407: 72-81.

[20] ZADIRIEV I, KRALKINA E, SAMOILOV V, et al. Plasma treatment for enhancement of the sorption capacity of carbon fabric [J]. *Plasma Science and Technology*, 2021, 23 (12): 125504.

[21] MUI T S M, SILVA L L G, PRYSIAZHNYI V, et al. Surface modification of aluminium alloys by atmospheric pressure plasma treatments for enhancement of their adhesion properties [J]. *Surface and Coatings Technology*, 2017, 312: 32-36.

[22] LI N Y Y, LI H G, WANG Q, et al. Effect of plasma surface treatment of aluminum alloy sheet on the properties of Al/Gf/PP laminates [J]. *Applied Surface Science*, 2020, 507: 145062.

[23] TSAI D C, CHANG Z C, CHEN E C, et al. Influence of plasma treatment on surface characteristics of aluminum alloy sheets and bonding performance of glass fiber-reinforced thermoplastic/Al composites [J]. *Materials*, 2023, 16(9): 3317.

[24] MOSKVINA V A, ASTAFUROVA E G, RAMAZANOV K N, et al. A role of initial microstructure in characteristics of the surface layers produced by ion-plasma treatment in CrNiMo austenitic stainless steel [J]. *Materials Characterization*, 2019, 153: 372-380.

[25] NI J R, MIN J Y, WAN H L, et al. Effect of adhesive type on mechanical properties of galvanized steel/SMC adhesive-bonded joints [J]. *International Journal of Adhesion and Adhesives*, 2020, 97: 102482.

[26] DANG J Q, ZOU F, CAI X J, et al. Experimental investigation on mechanical drilling of a newly developed CFRP/Al co-cured material [J]. *The International Journal of Advanced Manufacturing Technology*, 2020, 106(3): 993-1004.

[27] ZHANG H, DANG J Q, AN Q L, et al. Study on the drilling performances of a newly developed CFRP/invar co-cured material [J]. *Journal of Manufacturing Processes*, 2021, 66: 669-678.

[28] EL-SHEIKH S M, BARHOUM A, EL-SHERBINY S, et al. Preparation of superhydrophobic nanocalcite crystals using Box-Behnken design [J]. *Arabian Journal of Chemistry*, 2019, 12(7): 1479-1486.

[29] NEETHU B, THOLIA V, GHANGREKAR M M. Optimizing performance of a microbial carbon-capture cell using Box-Behnken design [J]. *Process Biochemistry*, 2020, 95: 99-107.

[30] SILVA T P, FERREIRA A N, DE ALBUQUERQUE F S, et al. Box-Behnken experimental design for the optimization of enzymatic saccharification of wheat bran [J]. *Biomass Conversion and Biorefinery*, 2022, 12 (12): 5597-5604.

[31] ZISMAN W A. Surface chemistry of plastics reinforced by strong fibers[J]. *Product R &D*, 1969, 8(2): 98-111.

[32] JONES F R. A review of interphase formation and design in fibre-reinforced composites [J]. *Journal of Adhesion Science and Technology*, 2010, 24(1): 171-202.

激光-等离子体协同处理增强 CFRP-6061 铝合金异质界面连接及服役性能研究

刘　杨#, 程乐乐#, 刘宇航, 焦子和, 张建新, 余木火, 孙泽玉*
东华大学 先进纤维材料全国重点实验室, 民用航空复合材料协同创新中心, 材料科学与工程学院, 上海 201620

摘　要: 碳纤维增强聚合物（carbon fiber reinforced polymer, CFRP）-铝合金兼具 CFRP 和铝合金的优点, 但由于两种材料性质不同, 二者的连接比较困难。该文利用响应面法优化了激光和等离子体处理 6061 铝合金（AA 6061）表面的工艺参数, 并在此参数下对 AA 6061 表面进行激光-等离子体协同处理, 之后采用共固化法制备 CFRP-AA 6061。通过滚筒剥离试验评估 CFRP-AA 6061 界面性能, 探究了不同服役环境条件、不同处理方式下, CFRP-AA 6061 的单层搭接剪切强度。研究发现激光处理最优参数为激光扫描线间距 0.115 mm、激光扫描速率 102.719 mm/s、激光频率 10.763 kHz, 此参数下 CFRP-AA 6061 平均剥离强度最高可达 103.76（N · mm)/mm;等离子体处理最优参数为气体流量 597.383 L/h、处理距离 5.821 mm、处理时间 173.132 s, 此参数下 CFRP-AA 6061 平均剥离强度最高可达 66.39（N · mm）/mm。两种处理方式在最优参数下的协同处理可使 CFRP-AA 6061 平均剥离强度达到 113.02（N · mm）/mm,并且在不同服役老化条件下表现出更优良的连接强度。该方法可为复合材料和金属异质连接界面处理提供参考。

关键词: 碳纤维增强聚合物; 6061 铝合金; 复合材料; 激光; 等离子体; 服役老化; 异质连接